www.cad-journal.net
Computer-Aided Design AND APPLICATIONS

Isogeometric Shape Optimization of Reissner-Mindlin Shell Structures for Maximizing Fundamental Eigenfrequency

Xiaoxiao Du[1], Zhihao Zhang[2], Zhaoyun Liu[3], Jiayi Li[4], Wei Wang[5], Gang Zhao[6]

[1]Beihang University, duxiaoxiao@buaa.edu.cn
[2]Beihang University, zhangzhih@buaa.edu.cn
[3]Beihang University, kkrylzy@buaa.edu.cn
[4]Beihang University, caulijiayi@163.com
[5]Beihang University, jrrt@buaa.edu.cn
[6]Beihang University, zhaog@buaa.edu.cn

Corresponding author: Gang Zhao, zhaog@buaa.edu.cn

Abstract. The fundamental eigenfrequency is a critical parameter that should be considered in the design of engineering structures. A lower fundamental eigenfrequency increases the susceptibility of a structure to large vibrations under low-frequency excitations, due to resonance phenomena. Isogeometric analysis offers an integrated workflow for computer-aided design (CAD) and finite element analysis (FEA) by directly utilizing spline-based CAD models for numerical simulations, thereby eliminating the need for traditional mesh generation. This seamless design-through-analysis process significantly facilitates structural shape optimization. In this paper, we develop a multi-patch isogeometric structural shape optimization framework for maximizing the fundamental eigenfrequency of shell structures. The Reissner-Mindlin shell theory is utilized for numerical simulation. A gradient-based optimization algorithm, combined with analytical sensitivity analysis, is employed to solve eigenfrequency optimization problems. Several numerical examples are presented to demonstrate the effectiveness of the proposed method.

Keywords: isogeometric shape optimization, Reissner-Mindlin shell, maximum fundamental eigenfrequency, analytical sensitivity
DOI: https://doi.org/10.14733/cadaps.2026.590-604

1 INTRODUCTION

Structural optimization serves as a systematic methodology to determine optimal structural parameters that maximize performance metrics while satisfying predefined constraints. This approach has been extensively applied in engineering design, including but not limited to automotive chassis design, aircraft wing airfoils, and

civil infrastructure such as bridge systems. Structural optimization techniques are broadly categorized into three primary domains: topology optimization, shape optimization, and size optimization. Topology optimization focuses on identifying the optimal material distribution pattern during the conceptual design phase, thereby defining the fundamental structural layout. Shape optimization subsequently enhances structural performance by refining the geometric boundaries derived from the initial topology. In contrast, size optimization operates at the final design stage, where it fine-tunes predefined geometric parameters (e.g., thickness or cross-sectional dimensions) to achieve localized performance improvements. In this paper we focus on the structural shape optimization.

The conventional shape optimization framework comprises three interdependent components: the design model for defining geometric parameters, the analysis model for simulating physical behavior, and the optimization model for governing parameter updates. Typically, the design model undergoes geometric simplification to generate an approximate analysis model for computational efficiency in numerical simulations (e.g., finite element method or boundary element method). The optimization model then establishes iterative feedback between the design and analysis models to drive performance improvements. However, this paradigm suffers from inherent limitations. First, the geometric approximation introduced during the conversion from design to analysis models accumulates errors and increases computational overhead. Second, the common practice of selecting discretized boundary nodes as design variables frequently leads to non-physical or non-manufacturable geometries. These challenges can be mitigated through isogeometric analysis (IGA) [18], which unifies the mathematical representations of design and analysis models using spline techniques, like non-uniform rational B-splines (NURBS) and T-splines [30, 7]. By eliminating geometric approximation and enabling direct parameter control, IGA streamlines the optimization loop while ensuring design integrity.

In recent years, isogeometric analysis (IGA) has demonstrated significant advantages in structural shape optimization, particularly for complex geometries. The foundational work by Wall et al. [33] pioneered the integration of IGA into structural optimization. Subsequent studies have expanded this paradigm across multiple dimensions, including optimization types (like topology [12, 42, 29], shape [36, 3, 41] and size [27, 15, 37] optimization), methodological components (like parametric modelling [23, 25, 32, 38] and algorithm development [21, 35, 24, 40]), and engineering applications [13, 14]. Notably, IGA exhibits unique strengths in free-form shell structure optimization [43, 34]. Its unified geometric representation eliminates shape approximation errors, which are innegligible in free-form shell structures, by maintaining exact consistency between design and analysis models. The inherent high-order continuity of spline-based formulations enhances numerical accuracy and convergence rates during sensitivity analysis. Furthermore, direct association of design variables with control points enables intuitive manipulation of free-form geometries.

Within the framework of isogeometric shell shape optimization, three dominant shell theories govern structural formulations: Kirchhoff-Love, Reissner-Mindlin, and solid-shell. Each theory exhibits distinct computational characteristics and application domains. The Kirchhoff-Love theory [20], requiring C^1-continuous shape functions, emerges as a computationally efficient choice for thin shells by employing only three displacement degrees of freedom (DOFs) per control point. It has garnered significant research interest in isogeometric shape optimization. [21, 6, 44]. In contrast, the Reissner-Mindlin theory relaxes continuity requirements to C^0, accommodating both thin and moderately thick shells at the expense of increased computational load due to six DOFs (three displacements and three rotations) per control point [4]. This approach enables effective shape optimization of complex thin-walled structures, particularly those composed of multiple patches [8, 45]. The solid-shell formulation demonstrates superior adaptability for shell structures exhibiting thickness variations or complex mechanical behaviors [5], and has been effectively implemented in thickness optimization studies [15]. These three theories exhibit complementary strengths, each demonstrating distinct advantages tailored to specific application scenarios.

The fundamental eigenfrequency represents a critical design parameter for engineering structures, as it directly governs their dynamic response under external excitations. Structures with lower fundamental eigenfrequencies exhibit heightened susceptibility to resonance-induced vibrations when subjected to low-frequency

loading, potentially compromising structural integrity and performance. Consequently, maximizing the fundamental eigenfrequency has become a key objective in vibration mitigation strategies during structural design. While topology optimization has been widely adopted for eigenfrequency maximization in recent decades [2, 39, 26, 17], shape optimization approaches for this purpose remain relatively underexplored. A key challenge lies in the difficulty of precise shape control within conventional FEA frameworks, where geometric discrepancies between design and analysis models often hinder optimization efficiency and accuracy. IGA addresses this limitation by enabling a seamless design-through-analysis process, significantly enhancing the robustness of structural shape optimization. For instance, Nagy et al. [28] explored the application of IGA to shape optimization of elastic arches for fundamental frequency maximization. Lei et al. [22] developed an IGA-based shape optimization framework for natural frequency problems using Kirchhoff-Love shell formulations, demonstrating the potential of IGA in overcoming traditional geometric limitations.

This study investigates isogeometric shape optimization for shell structures using Reissner-Mindlin shell formulations, which offer robust and accurate solutions for complex shell geometries, making them particularly suitable for practical engineering applications. Building upon our prior work on isogeometric structural shape optimization with compliance minimization as the objective [8], we extend the methodology to eigenfrequency optimization. A gradient-based optimization framework, integrated with analytical sensitivity analysis, is developed to efficiently solve the eigenfrequency maximization problem. To enhance computational efficiency, a multi-level geometric representation is adopted, where a coarse model facilitates shape updates while a refined model ensures high-fidelity isogeometric analysis. The proposed approach is validated through a series of numerical examples, demonstrating its effectiveness in achieving optimal shell designs with improved dynamic performance. In particular, a stiffened cylindrical shell modeled with nine NURBS patches is analyzed, illustrating the potential of the proposed multi-patch shape optimization method for practical engineering applications.

2 FREE VIBRATION ANALYSIS OF REISSNER-MINDLIN SHELL

A multi-patch isogeometric Reissner-Mindlin shell method is employed for the numerical simulation of shell structures. The deformation behavior of shell structures is assumed to occur within the regime of small displacements and small rotations. A shell structure can be represented by its middle surface as follows:

$$\boldsymbol{x}(\xi,\eta,\zeta) = \tilde{\boldsymbol{x}}(\xi,\eta) + \frac{t}{2}\zeta \boldsymbol{n}(\xi,\eta), \tag{1}$$

in which $\tilde{\boldsymbol{x}}(\xi,\eta)$ denotes the middle surface represented by NURBS patches; t is the thickness of the shell; $\boldsymbol{n}(\xi,\eta)$ indicates the unit normal vector; $\zeta \in [-1,1]$ is the parameter along the thickness direction.

The displacement of the shell structure is then written as [1]

$$\boldsymbol{u}(\xi,\eta,\zeta) = \tilde{\boldsymbol{u}}(\xi,\eta) + \frac{t}{2}\zeta \left[\tilde{\boldsymbol{\theta}}(\xi,\eta) \times \boldsymbol{n}(\xi,\eta)\right], \tag{2}$$

where $\tilde{\boldsymbol{u}}(\xi,\eta)$ and $\tilde{\boldsymbol{\theta}}(\xi,\eta)$ denote the displacements and rotations of the middle surface. Using NURBS basis functions to interpolate the nodal displacements and rotations defined at control points, Eq. (2) can be rewritten as

$$\boldsymbol{u}(\xi,\eta,\zeta) = \sum_{i=0}^{n_{cp}} R_i(\xi,\eta) \left\{ \tilde{\boldsymbol{u}}_i + \frac{t}{2}\zeta \left[\tilde{\boldsymbol{\theta}}_i \times \boldsymbol{n}(\xi,\eta)\right] \right\}, \tag{3}$$

in which $\tilde{\boldsymbol{u}}_i = [u_i, v_i, w_i]^T$ and $\tilde{\boldsymbol{\theta}}_i = [\theta_{xi}, \theta_{yi}, \theta_{zi}]^T$ represent the three displacements and three rotations defined at the i-th control point [11].

Arranging the translational displacements $\tilde{\boldsymbol{u}}_i$ and rotational displacements $\tilde{\boldsymbol{\theta}}_i$ into a 6×1 vector as $\bar{\boldsymbol{u}}_i$, the strain vector $\boldsymbol{\epsilon}$ in Voigt form can be given by

$$\boldsymbol{\epsilon} = [\epsilon_{xx}, \epsilon_{yy}, \epsilon_{zz}, 2\epsilon_{xy}, 2\epsilon_{yz}, 2\epsilon_{xz}]^T = \sum_{i=0}^{n_{cp}} \boldsymbol{B}_i \bar{\boldsymbol{u}}_i = \boldsymbol{B}\boldsymbol{u}, \tag{4}$$

where $\boldsymbol{B}$ denotes the strain-displacement matrix and its component $\boldsymbol{B}_i$ is defined as

$$\boldsymbol{B}_i = \begin{bmatrix} R_{i,x} & 0 & 0 & 0 & (\bar{R}_i n_3)_{,x} & -(\bar{R}_i n_2)_{,x} \\ 0 & R_{i,y} & 0 & -(\bar{R}_i n_3)_{,y} & 0 & (\bar{R}_i n_1)_{,y} \\ 0 & 0 & R_{i,z} & (\bar{R}_i n_2)_{,z} & -(\bar{R}_i n_1)_{,z} & 0 \\ R_{i,y} & R_{i,x} & 0 & -(\bar{R}_i n_3)_{,x} & (\bar{R}_i n_3)_{,y} & (\bar{R}_i n_1)_{,x} - (\bar{R}_i n_2)_{,y} \\ 0 & R_{i,z} & R_{i,y} & (\bar{R}_i n_2)_{,y} - (\bar{R}_i n_3)_{,z} & -(\bar{R}_i n_1)_{,y} & (\bar{R}_i n_1)_{,z} \\ R_{i,z} & 0 & R_{i,x} & (\bar{R}_i n_2)_{,x} & (\bar{R}_i n_3)_{,z} - (\bar{R}_i n_1)_{,x} & -(\bar{R}_i n_2)_{,z} \end{bmatrix}, \tag{5}$$

with $\bar{R}_i = \zeta R_i h/2$.

The solution for the free vibration analysis of shell structures, can be obtained by solving the following stiffness equation

$$(\boldsymbol{K} + \lambda_n \boldsymbol{M})\boldsymbol{u}_n = \boldsymbol{0}. \tag{6}$$

where $\boldsymbol{K}$ and $\boldsymbol{M}$ denote the stiffness matrix and the mass matrix, respectively; λ_n is the n-th frequency parameter and $\boldsymbol{u}_n$ is the eigenvector corresponding to λ_n. The eigenvector $\boldsymbol{u}_n$ is normalized using the mass matrix with $\boldsymbol{u}_n^T \boldsymbol{M} \boldsymbol{u}_n = 1$. Assuming that the shell structure is constructed by n_{pth} NURBS patches, $\boldsymbol{K}$ and $\boldsymbol{M}$ can be computed as

$$\boldsymbol{K} = \sum_{I=1}^{n_{pth}} \int_{\Omega_I} \left(\boldsymbol{B}^T \boldsymbol{D} \boldsymbol{B}\right) d\Omega_I, \quad \boldsymbol{M} = \sum_{I=1}^{n_{ph}} \int_{\Omega_I} \left(\rho \boldsymbol{N}^T \boldsymbol{N}\right)\ d\Omega_I. \tag{7}$$

in which $\boldsymbol{D}$ represents the global constitutive matrix; $\boldsymbol{N}$ is the shape function matrix; Ω_I indicates the physical space of I-th NURBS patch. For a detailed derivation of the isogeometric Reissner-Mindlin shell formulations, the reader is referred to [10, 11].

3 ISOGEOMETRIC SHAPE OPTIMIZATION

The fundamental eigenfrequency, λ_1, can be maximized by minimizing the objective function $f = 1/\lambda_1$. However, this objective function is discontinuous and may not be differentiable, which can adversely affect the convergence of the optimization process. Furthermore, optimizing a single eigenfrequency may lead to mode switching issues. To address these challenges, a multi-eigenfrequency objective function, as proposed in [16], is adopted:

$$f(\boldsymbol{h}) = \left\{ \sum_{i=1}^{n_\lambda} \left(\frac{1}{\lambda_i(\boldsymbol{h})} \right)^{\alpha} \right\}^{1/\alpha}. \tag{8}$$

where $\boldsymbol{h}$ denotes the set of design variables. Let $\boldsymbol{h} = (h_1, h_2, \cdots, h_{n_d})$, the shape optimization of a shell structure can be expressed as:

$$\begin{aligned} find \quad & \boldsymbol{h} \in \mathbb{R}^3 \\ min \quad & f = f(\boldsymbol{h}) \\ s.t. \quad & [\boldsymbol{K}(\boldsymbol{h}) + \lambda_n \boldsymbol{M}(\boldsymbol{h})]\, \boldsymbol{u}_n = \boldsymbol{0}, \\ & g(\boldsymbol{h}) = S(\boldsymbol{h})/S_0 - \gamma \leq 0, \\ & h_i^{min} \leq h_i \leq h_i^{max},\ i = 1, \cdots, n_d \end{aligned} \tag{9}$$

in which $S(\boldsymbol{h})$ is the area of the middle surface of the shell structure for a design set $\boldsymbol{h}$; S_0 denotes the initial area; γ is the prescribed area fraction; h_i^{min} and h_i^{max} denote the minimum and maximum limits of the i-th design variable h_i.

Within the framework of isogeometric shape optimization, a multi-level representation of the geometric model can be employed, with a coarse model used for design purposes and a denser model for analysis. The design variables are associated with the control points of the coarse design model. Let $\boldsymbol{P}$ and $\boldsymbol{Q}$ denote the control point vectors of the design model and the analysis model, respectively. A refinement or transformation matrix $\boldsymbol{R}$ is constructed based on the knot insertion and degree elevation algorithms of the NURBS technique, such that $\boldsymbol{Q} = \boldsymbol{R}\boldsymbol{P}$. Utilizing the adjoint method, the sensitivity of the k-th eigenvalue λ_k with respect to the dense control points $\boldsymbol{Q}$ can be computed by:

$$\frac{d\lambda_k}{d\boldsymbol{Q}} = \boldsymbol{u}_k^T \left(\frac{\partial \boldsymbol{K}}{\partial \boldsymbol{Q}} - \lambda_k \frac{\partial \boldsymbol{M}}{\partial \boldsymbol{Q}} \right) \boldsymbol{u}_k. \tag{10}$$

The differentiation of the stiffness matrix $\boldsymbol{K}$ with respect to the control points $\boldsymbol{Q}$ is written as

$$\frac{\partial \boldsymbol{K}}{\partial \boldsymbol{Q}} = \int_{\bar{\Omega}} \left(\frac{\partial \boldsymbol{B}^T}{\partial \boldsymbol{Q}} \boldsymbol{D}\boldsymbol{B} + \boldsymbol{B}^T \frac{\partial \boldsymbol{D}}{\partial \boldsymbol{Q}} \boldsymbol{B} + \boldsymbol{B}^T \boldsymbol{D} \frac{\partial \boldsymbol{B}}{\partial \boldsymbol{Q}} \right) |\boldsymbol{J}| d\bar{\Omega} + \int_{\bar{\Omega}} \left(\boldsymbol{B}^T \boldsymbol{D}\boldsymbol{B} \right) \frac{\partial |\boldsymbol{J}|}{\partial \boldsymbol{Q}} d\bar{\Omega}, \tag{11}$$

while the differentiation of the mass matrix with respect to the control points, $\partial \boldsymbol{M}/\partial \boldsymbol{Q}$, can be derived as

$$\frac{\partial \boldsymbol{M}}{\partial \boldsymbol{Q}} = \rho \int_{\bar{\Omega}} \left\{ \frac{\partial \boldsymbol{N}^T}{\partial \boldsymbol{Q}} \boldsymbol{N} |\boldsymbol{J}| + \boldsymbol{N}^T \frac{\partial \boldsymbol{N}}{\partial \boldsymbol{Q}} |\boldsymbol{J}| + \boldsymbol{N}^T \boldsymbol{N} \frac{\partial |\boldsymbol{J}|}{\partial \boldsymbol{Q}} \right\} d\bar{\Omega}, \tag{12}$$

where $|\boldsymbol{J}|$ is the determinant of the Jacobian matrix and $\bar{\Omega}$ denotes the parametric space corresponding to the physical space Ω. The differentiation of the coarse control points $\boldsymbol{P}$ with respect to the design variable h_i is specified. Considering the refinement matrix and the differentiating chain rule, the sensitivity of the multi-eigenfrequency objective function, as given in Eq. (8), takes the form:

$$\frac{df}{dh_i} = \frac{\partial f}{\partial h_i} + \frac{\partial f}{\partial \lambda_k} \frac{\partial \lambda_k}{\partial \boldsymbol{Q}} \boldsymbol{R} \frac{\partial \boldsymbol{P}}{\partial h_i}. \tag{13}$$

At this stage, the sensitivity can be explicitly derived. The open-source framework, NLIGA [9], can be utilized for numerical implementation, in conjunction with the open-source library NLOPT [19, 31] for solving the optimization problem.

4 NUMERICAL EXAMPLES

4.1 A Square Plate

We first consider the shape optimization of a square plate under area constraints. The plate, with its left and right edges fixed as depicted in Fig. 1(a), has a side length of 10m and a thickness of 0.5m. The

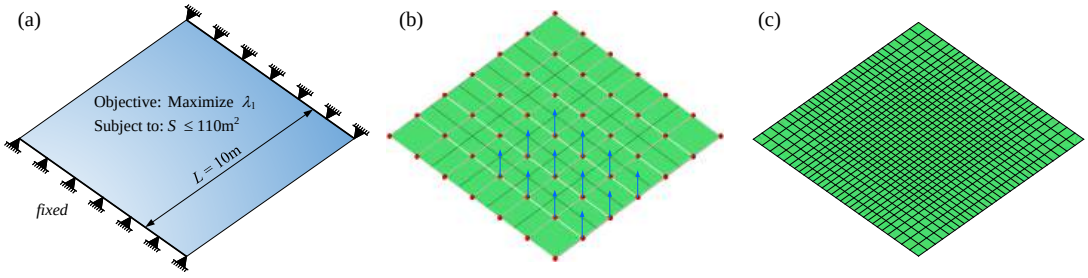

Figure 1: Schematic diagram and geometrical modeling of the square plate. (a)Problem definition; (b) Design model with 5×5 bi-quadratic NURBS elements and 7×7 control points; (c) Analysis model with 30×30 bi-quadratic NURBS elements.

material properties are defined as follows: Young's modulus $E = 30$MPa, Poisson's ratio $\nu = 0.3$, and density $\rho = 2500$ Kg/m^3. The objective is to maximize the fundamental frequency of the plate under the area constraint $S \leq 110\text{m}^2$.

As shown in Fig. 1(b), the initial design model discretizes the square plate using 5×5 biquadratic NURBS elements, with 7×7 control points defined in the $x - y$ plane. The vertical movements (along the z-axis) of all free control points (excluding those on the fixed edges) are selected as design variables. Consequently, the design update can be expressed as:

$$\boldsymbol{P}_i^{new} = \boldsymbol{P}_i + h_i \boldsymbol{e}_3. \tag{14}$$

The optimization process involves 35 design variables. The design model is refined into an analysis model using 30×30 bi-quadratic NURBS elements and 32×32 control points for vibration analysis, as illustrated in Fig 1(c).

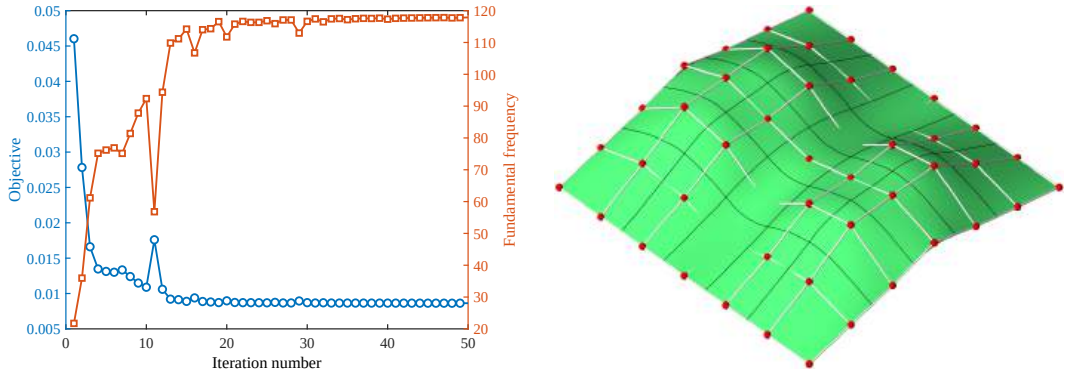

Figure 2: Optimization history and optimized shape of the square plate. Left: Optimization history of the objective function and the first-order eigenfrequency. Right: Optimized shape of the square plate at the 50th iteration.

Figure 2(a) shows the optimization histories of the objective function (left vertical axis) and the fundamental eigenfrequency (right vertical axis) of the square plate. Both the objective function and eigenfrequency converge to stable values after 20 iterations. The optimized plate geometry is shown in Fig. 2(b). For quantitative analysis, Table 1 compares the first eight eigenfrequencies of the initial and optimized configurations.

Table 1: The first eight eigenfrequencies of the square plate, both before and after shape optimization, using IGA and FEA with ABAQUS.

Mode Sequence	1	2	3	4	5	6	7	8
Initial Model (IGA)	12.989	18.112	48.286	94.520	112.59	158.89	186.56	343.98
Initial Model (FEA)	12.970	18.070	48.165	94.326	112.28	158.61	185.98	343.02
Optimized Model (IGA)	117.88	117.97	118.06	124.28	129.70	194.55	292.34	307.98
Optimized Model (FEA)	116.67	117.32	118.20	123.41	129.09	191.52	288.98	304.73
Increase (IGA, %)	807.54	551.34	144.50	31.485	15.197	22.443	56.700	-10.466

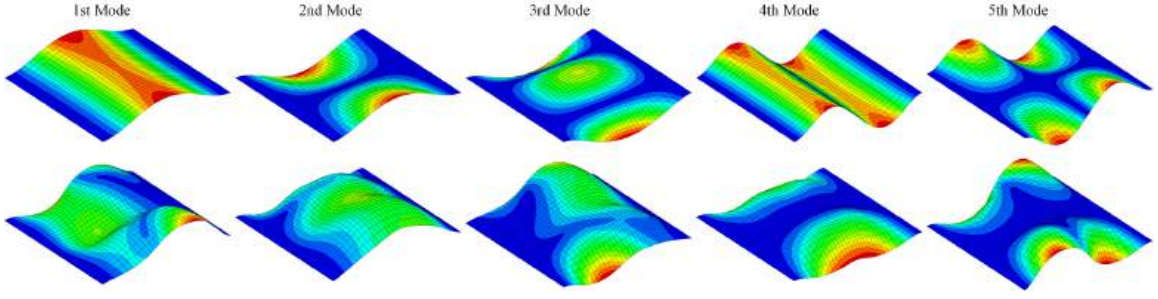

Figure 3: The first five mode shapes of the square plate with the upper panel depicting the initial design and the lower panel illustrating the optimized design.

To validate the vibration analysis methodology, results from the proposed approach are compared with finite element analysis (FEA) performed using ABAQUS. In the ABAQUS model, the plate is discretized into 10,300 quadratic S8R shell elements with 31,307 nodes. The first eight eigenfrequencies obtained via isogeometric analysis (IGA) and FEA exhibit excellent agreement for both initial and optimized configurations. Notably, the optimized plate achieves a nine-fold increase in fundamental eigenfrequency compared to the initial design. However, the eighth eigenfrequency exhibits a 10.466% reduction after shape optimization. Fig. 3 presents the first five modes shapes of the square plate with the upper panel depicting the initial design and the lower panel illustrating the optimized design.

Finally, we also examine the optimization history of the design variables. Figure 4(a) illustrates the selected variables for analysis: $h_2, h_6, h_{30}, h_{34}, h_{15}, h_{21}$. As expected, due to the symmetry of the square plate and its boundary conditions, the variables h_2, h_6, h_{30} and h_{34} exhibit similar trends, as do h_{15} and h_{21}, as given in Fig. 4(b). This suggests that design variables will exhibit similar variation patterns when the initial geometry and boundary conditions are symmetric. Consequently, the optimized shape preserves these symmetric properties, as evident in the final design shown in Fig. 2(b).

4.2 A Cylindrical Shell

In this section, the shape optimization of a cylindrical shell is investigated. The geometric parameters, as illustrated in Fig. 5(a), are defined with $L = 60$m and $R = 10$m. The material properties are the same with those given for the previous example. The thickness of the shell takes $t = 0.5$m. The left end boundary is clamped.

The design model is represented by 16 quadratic elements, as depicted in Fig. 5(b). Along the length direction of the cylindrical shell, which aligns with the x-axis, there are six layers of control points. Each layer

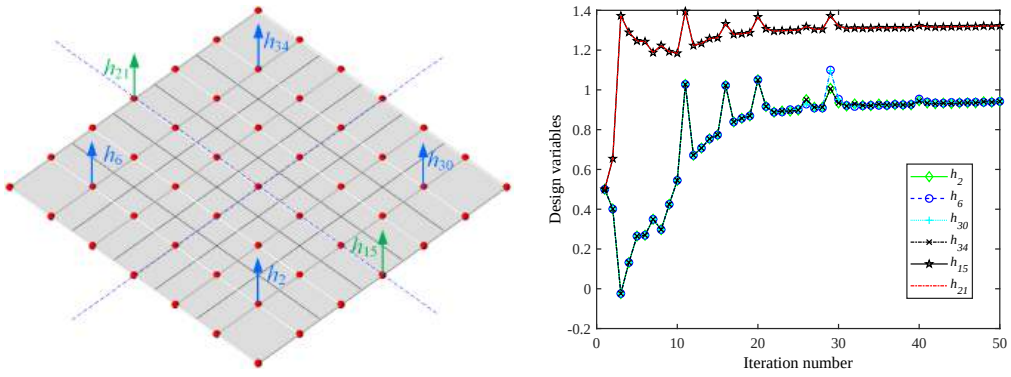

Figure 4: Optimization history of design variables $h_2, h_6, h_{30}, h_{34}, h_{15}, h_{21}$. Left: label of the design variables. Right: Optimization history.

comprises nine control points. The design variable is assigned to the i-th layer of control points. Consequently, the derivative of the j-th layer control point $\mathbf{P}_k^j$, as illustrated in Fig. 5(c), with respect to the design variable h_i, can be explicitly expressed as:

$$\begin{aligned}
&\frac{\partial \boldsymbol{P}_1^j}{\partial h_i} = \frac{\partial \boldsymbol{P}_9^j}{\partial h_i} = [0,1,0], \quad \frac{\partial \boldsymbol{P}_2^j}{\partial h_i} = \left[0, \frac{\sqrt{2}}{2}, \frac{\sqrt{2}}{2}\right], \quad \frac{\partial \boldsymbol{P}_3^j}{\partial h_i} = [0,0,1], \quad \frac{\partial \boldsymbol{P}_4^j}{\partial h_i} = \left[0, -\frac{\sqrt{2}}{2}, \frac{\sqrt{2}}{2}\right], \\
&\frac{\partial \boldsymbol{P}_5^j}{\partial h_i} = [0,-1,0], \quad \frac{\partial \boldsymbol{P}_6^j}{\partial h_i} = \left[0, -\frac{\sqrt{2}}{2}, -\frac{\sqrt{2}}{2}\right], \quad \frac{\partial \boldsymbol{P}_7^j}{\partial h_i} = [0,0,-1], \quad \frac{\partial \boldsymbol{P}_8^j}{\partial h_i} = \left[0, \frac{\sqrt{2}}{2}, -\frac{\sqrt{2}}{2}\right].
\end{aligned} \tag{15}$$

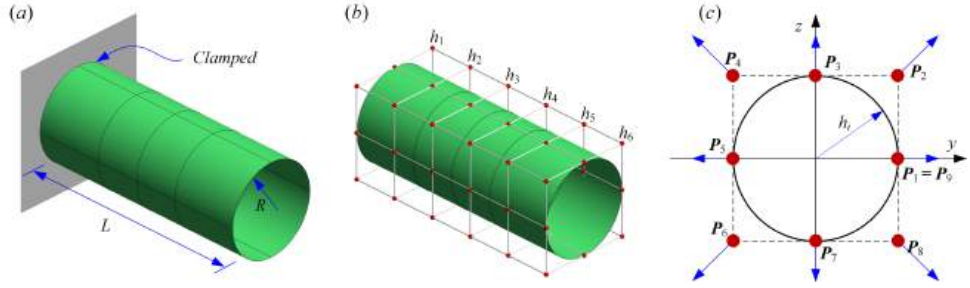

Figure 5: Geometrical modeling of a cylindrical shell. (a)Geometrical dimensions; (b) Design model; (c) circumferential parametrization using the design variable.

We first examine the convergence of the eigenfrequencies for the initial cylindrical shell without shape optimization. The cylindrical shell is progressively refined into 4×4, 8×8, 12×12, 16×16, 24×24, 32×32, and 48×48 bi-quadratic elements. As illustrated in Fig. 6, it is observed that the first three eigenfrequencies converge to relatively stable values upon refinement to 24×24 elements. Conservatively, the refinement of 32×32 elements is adopted as the dense analysis model for subsequent shape optimization.

The design variables are constrained to the range $[-5, 5]$, and the area is restricted to be smaller than the initial area throughout the shape optimization process. Fig. 7 illustrates the history of the shape optimization process, depicting both the objective function and the first-order eigenfrequency of the cylindrical shell. Convergence is achieved for both metrics after fifteen iterations. Notably, the radius of the left-end circle increases

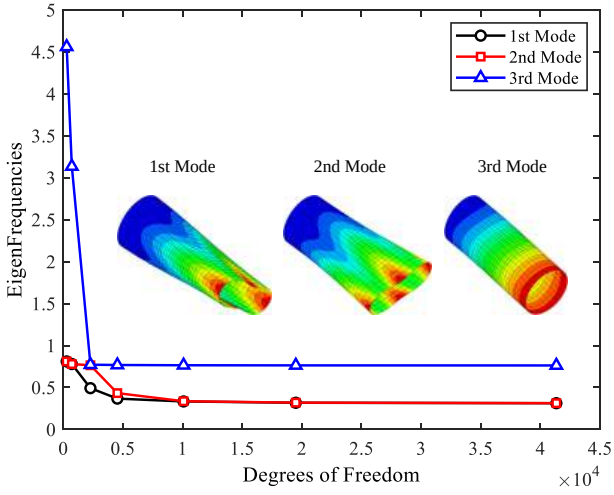

Figure 6: Convergence of the first three eigenfrequencies and corresponding mode shapes of the initial cylindrical shell, without shape optimization.

from 5 m to 10 m, while the radius of the right-end circle decreases from 10 m to 5.6475 m. Fig. 8 presents the first twelve mode shapes of the optimized cylindrical shell. For quantitative comparison, Table 2 lists the first eight eigenfrequencies of the initial and optimized models, revealing a significant increase following shape optimization; in particular, the first-order eigenfrequency rises by 568.60%, from 0.3115 to 2.0827.

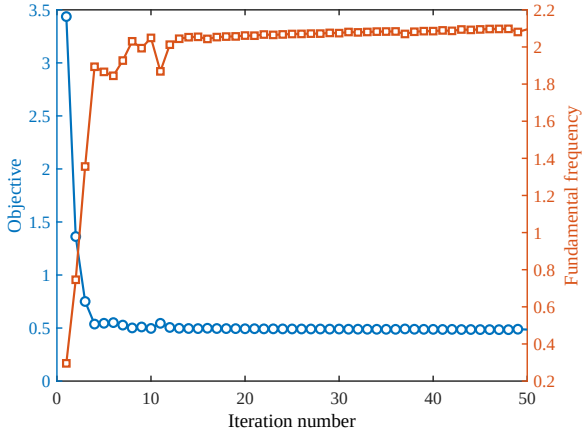

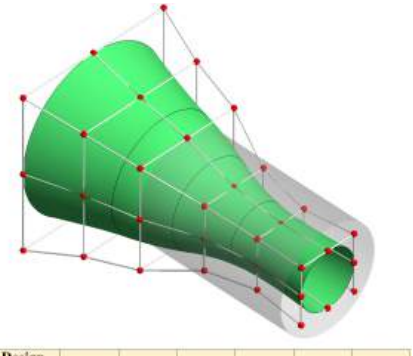

Design variable	h_1	h_2	h_3	h_4	h_5	h_6
Value at 50th step	5.0000	2.0617	0.0302	-3.6695	-5.0000	-4.3525

Figure 7: Left: Optimization history of the objective function and the first-order eigenfrequency. Right: Optimized cylindrical shell at the 50th iteration, along with the corresponding design variables.

4.3 A Stiffened Cylindrical Shell

In this example, we extend the optimization of the cylindrical shell investigated previously by incorporating eight longitudinal stiffeners as illustrated in Fig. 9(a). The stiffened shell maintains identical geometric parameters (radius and length) and material properties as the baseline configuration in the prior study. The stiffeners

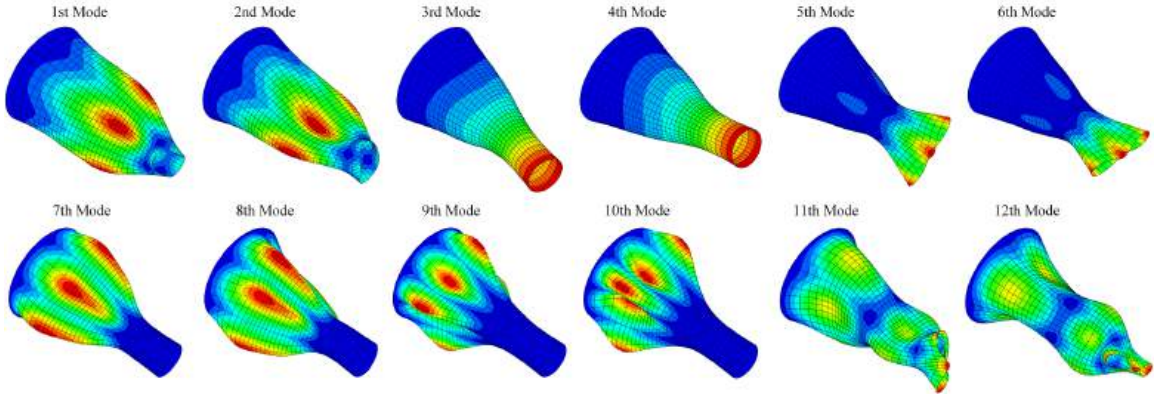

Figure 8: The first ten mode shapes of the optimized cylindrical shell.

Table 2: The first eight eigenfrequencies of the cylindrical shell, both before and after shape optimization.

Mode Sequence	1	2	3	4	5	6	7	8
Initial Model	0.3115	0.3115	0.7624	0.7624	1.6208	1.6208	2.6821	2.6821
Optimized Model	2.0827	2.0827	2.0937	2.0937	3.8159	3.8159	4.7250	4.7250
Increase (%)	568.60	568.60	174.62	174.62	135.43	135.43	76.168	76.168

maintain a constant width of $T = R/8$ while achieving full-length geometric continuity with the host shell. The design model employs nine biquadratic NURBS patches, with the following parametric discretization: (a) The host cylindrical shell consists of 8×4 quadratic elements and 16×6 control points; (b) Each stiffener consists of 4×1 quadratic elements and 6×3 control points as illustrated in Fig. 9(b). Note that the control points of the stiffeners and the host cylindrical shell along the interfaces exactly coincide with each other. The design variables retain identical specifications to those defined in the previous example and constrained within [-5,5]. For high-fidelity analysis, the design model undergoes h-refinement with 24×24 quadratic elements for the cylindrical shell and 24×3 for each stiffener as given in Fig. 9(c).

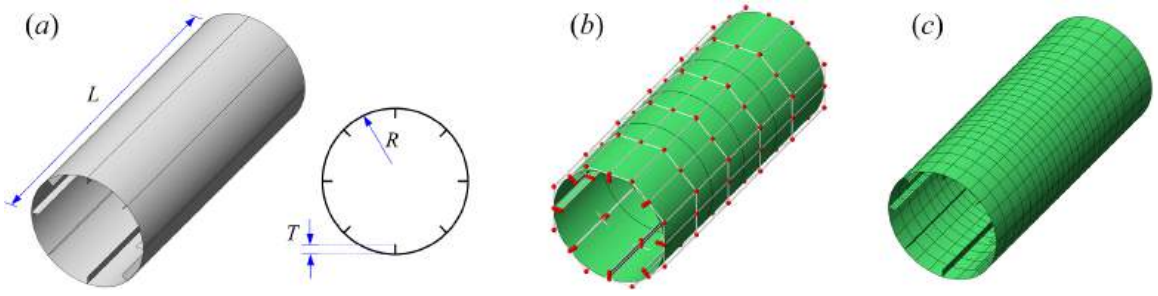

Figure 9: The parametric modelling of the stiffened cylindrical shell. (a) Schematic diagram, (b) Design model and (c) Analysis model

Fig. 10(a) presents the convergence history of the objective function and first-order eigenfrequency, along with the geometrically optimized stiffened cylindrical shell. The optimized host shell configuration exhibits

close alignment with the reference results from the prior study. At final convergence, the six design variables attain values of 5.0000, 2.2576, -0.8639, -3.3599, -5.0000, demonstrating boundary-driven behavior: the fixed-edge radius reaches its upper constraint limit, while the free-edge radius converges to its lower bound. The evolutionary trajectories of these design variables, plotted in Fig. 10(b), reveal rapid stabilization within the optimization process. As quantified in Table 3, the fundamental eigenfrequency undergoes a 536.56% enhancement, increasing from 0.2839 to 1.8070. Comparative modal analysis in Fig. 11 demonstrates excellent consistency between isogeometric analysis (IGA) and finite element analysis (FEA) predictions for the 2nd, 4th, 6th, 8th, and 10th vibrational modes of the optimized structure.

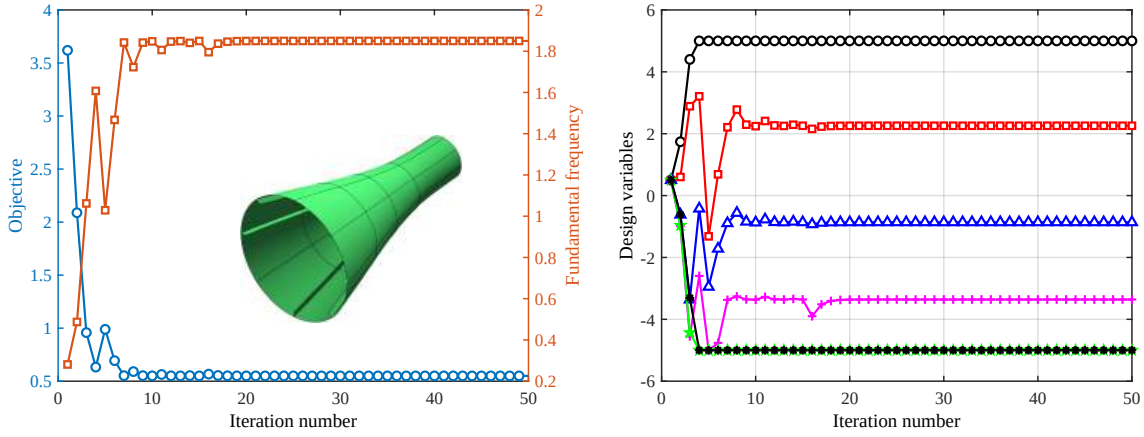

Figure 10: Left: Optimization history of the objective function and the first-order eigenfrequency, and the stiffened cylindrical shell after shape optimization. Right: Optimization history of the six design variables.

Table 3: The first eight eigenfrequencies of the stiffened cylindrical shell, both before and after shape optimization.

Mode Sequence	1	2	3	4	5	6	7	8
Initial Model	0.2839	0.2839	0.7184	0.7184	1.4750	1.4750	2.4229	2.4229
Optimized Model	1.8070	1.8070	1.8484	1.8484	3.3525	3.3525	3.4646	3.4646
Increase (%)	536.56	536.56	157.29	157.29	127.29	127.29	42.992	42.992

5 CONCLUSIONS

This study presents a systematic isogeometric shape optimization framework for fundamental eigenfrequency maximization in thin-shell structures by using the Reissner-Mindlin shell formulations. A multi-level geometric parametrization strategy is developed to resolve the inherent parametric consistency requirements between design parametrization and analysis-suitable discretization. Governing sensitivity operators are rigorously derived using analytic differentiation techniques to enable gradient-based optimization. Numerical experiments demonstrate significant eigenfrequency enhancements, with three examples achieving fundamental mode enhancements of 807.54%, 568.60% and 536.56% respectively. Notably, the optimized configurations preserve geometric symmetry when initialized with symmetric design parameterizations and constrained boundary con-

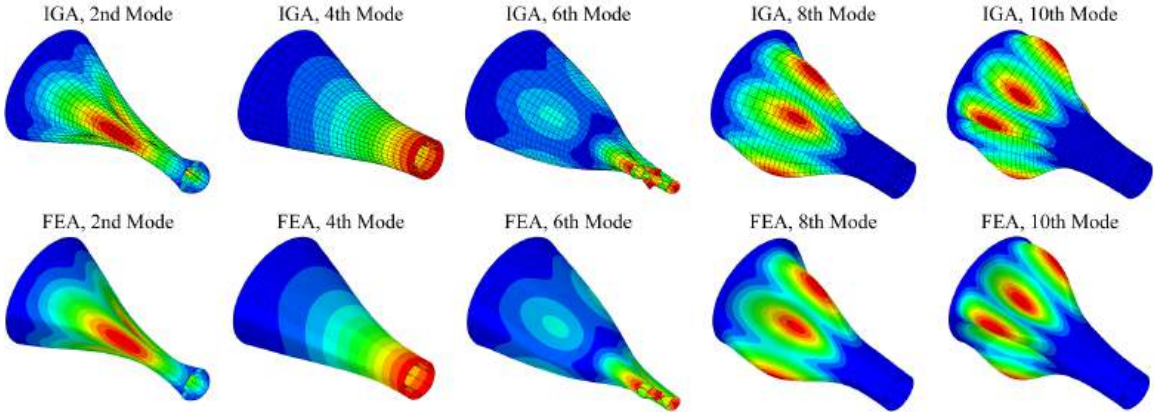

Figure 11: The 2nd, 4th, 6th, 8th and 10th mode shapes of the optimized stiffened cylindrical shell obtained by using IGA (the first layer) and FEA (the second layer).

ditions. These results collectively validate the method's efficacy in addressing fundamental frequency amplification in thin-walled structures.

In practical engineering shape optimization applications, various geometric and structural constraints, such as curvature, displacement and stress, are often critical. While this study considers only volume constraints, the proposed framework can be extended to incorporate additional constraint types, which presents a promising direction for future research. Moreover, the current implementation of analytical sensitivity analysis, although precise, is computationally demanding. Efficiency improvements could be achieved through the use of reduced integration schemes and accelerated stiffness matrix assembly techniques. Finally, expanding the method to handle more complex structural configurations and large displacement scenarios would significantly enhance its applicability and robustness in real-world engineering problems.

ACKNOWLEDGEMENTS

This research is partially supported by National Key Research and Development Program of China (Project No. 2023YFB3309000), Beijing Natural Science Foundation of China (Project No. 4242025), National Natural Science Foundation of China (Project Nos. 52175213 and 62102012) and Young Elite Scientists Sponsorship Program by CAST (Project No. 2022QNRC001).

Xiaoxiao Du https://orcid.org/0000-0002-2324-1005

REFERENCES

[1] Adam, C.; Bouabdallah, S.; Zarroug, M.; Maitournam, H.: Improved numerical integration for locking treatment in isogeometric structural elements. Part II: Plates and shells. Computer Methods in Applied Mechanics and Engineering, 284, 106–137, 2015. http://doi.org/10.1016/j.cma.2014.07.020.

[2] Allaire, G.; Aubry, S.; Jouve, F.: Eigenfrequency optimization in optimal design. Computer Methods in Applied Mechanics and Engineering, 190(28), 3565–3579, 2001. http://doi.org/10.1016/S0045-7825(00)00284-X.

[3] Bandara, K.; Cirak, F.: Isogeometric shape optimisation of shell structures using multiresolution subdivision surfaces. Computer-Aided Design, 95, 62–71, 2018. http://doi.org/10.1016/j.cad.2017.09.006.

[4] Benson, D.J.; Bazilevs, Y.; Hsu, M.C.; Hughes, T.: Isogeometric shell analysis: the Reissner–Mindlin shell. Computer Methods in Applied Mechanics and Engineering, 199(5-8), 276–289, 2010. http://doi.org/10.1016/j.cma.2009.05.011.

[5] Bouclier, R.; Elguedj, T.; Combescure, A.: Efficient isogeometric NURBS-based solid-shell elements: Mixed formulation and B-method. Computer Methods in Applied Mechanics and Engineering, 267, 86–110, 2013. http://doi.org/10.1016/j.cma.2013.08.002.

[6] Cai, S.; Zhang, H.; Zhang, W.: An integrated design approach for simultaneous shape and topology optimization of shell structures. Computer Methods in Applied Mechanics and Engineering, 415, 116218, 2023. http://doi.org/10.1016/j.cma.2023.116218.

[7] Du, X.; Lei, S.; Huang, Z.; Wang, W.; Zhao, G.: Seamless integration of design and analysis for architected shell structures using unstructured T-splines. Computer Methods in Applied Mechanics and Engineering, 435, 117619, 2025. http://doi.org/10.1016/j.cma.2024.117619.

[8] Du, X.; Li, J.; Wang, W.; Zhao, G.; Liu, Y.; Zhang, P.: Isogeometric shape optimization of reissner–mindlin shell with analytical sensitivity and application to cellular sandwich structures. Computer-Aided Design, 173, 103728, 2024. http://doi.org/10.1016/j.cad.2024.103728.

[9] Du, X.; Zhao, G.; Wang, W.; Guo, M.; Zhang, R.; Yang, J.: NLIGA: A MATLAB framework for nonlinear isogeometric analysis. Computer Aided Geometric Design, 80, 101869, 2020. http://doi.org/10.1016/j.cagd.2020.101869.

[10] Du, X.; Zhao, G.; Wang, W.; Liu, Y.; Zhang, P.; Han, P.; Cheng, H.: Parametric modeling and simulation of a simplified horizontal tail under the framework of isogeometric analysis. Computer-Aided Design & Applications, 21, 635–645, 2024. http://doi.org/10.14733/cadaps.2024.635-645.

[11] Du, X.; Zhao, G.; Zhang, R.; Wang, W.; Yang, J.: Numerical implementation for isogeometric analysis of thin-walled structures based on a Bézier extraction framework: nligaStruct. Thin-Walled Structures, 180, 109844, 2022. http://doi.org/10.1016/j.tws.2022.109844.

[12] Gao, J.; Xiao, M.; Zhang, Y.; Gao, L.: A comprehensive review of isogeometric topology optimization: methods, applications and prospects. Chinese Journal of Mechanical Engineering, 33, 1–14, 2020. http://doi.org/10.1186/s10033-020-00503-w.

[13] Guerder, M.; Duval, A.; Elguedj, T.; Dam, D.: Volumetric embedded entities for the isogeometric analysis of complex structures. Computer Methods in Applied Mechanics and Engineering, 417, 116426, 2023. http://doi.org/10.1016/j.cma.2023.116426.

[14] Guerder, M.; Duval, A.; Elguedj, T.; Feliot, P.; Touzeau, J.: Isogeometric shape optimisation of volumetric blades for aircraft engines. Structural and Multidisciplinary Optimization, 65(3), 86, 2022. http://doi.org/10.1007/s00158-021-03090-z.

[15] Hirschler, T.; Bouclier, R.; Duval, A.; Elguedj, T.; Morlier, J.: Isogeometric sizing and shape optimization of thin structures with a solid-shell approach. Structural and Multidisciplinary Optimization, 59, 767–785, 2019. http://doi.org/10.1007/s00158-018-2100-6.

[16] Hirschler, T.; Bouclier, R.; Duval, A.; Elguedj, T.; Morlier, J.: A new lighting on analytical discrete sensitivities in the context of isogeometric shape optimization. Archives of Computational Methods in Engineering, 28(4), 2371–2408, 2021. http://doi.org/10.1007/s11831-020-09458-6.

[17] Hu, T.; Wang, Y.; Zhang, H.; Li, H.; Ding, X.; Izui, K.; Nishiwaki, S.: Topology optimization of coated structures with layer-wise graded lattice infill for maximizing the fundamental eigenfrequency. Computers & Structures, 271, 106861, 2022. http://doi.org/10.1016/j.compstruc.2022.106861.

[18] Hughes, T.J.; Cottrell, J.A.; Bazilevs, Y.: Isogeometric analysis: CAD, finite elements, NURBS, exact geometry and mesh refinement. Computer methods in applied mechanics and engineering, 194(39-41), 4135–4195, 2005. http://doi.org/10.1016/j.cma.2004.10.008.

[19] Johnson, S.G.: The NLopt nonlinear-optimization package. https://github.com/stevengj/nlopt, 2007.

[20] Kiendl, J.; Bletzinger, K.U.; Linhard, J.; Wüchner, R.: Isogeometric shell analysis with Kirchhoff–Love elements. Computer methods in applied mechanics and engineering, 198(49-52), 3902–3914, 2009. http://doi.org/10.1016/j.cma.2009.08.013.

[21] Kiendl, J.; Schmidt, R.; Wüchner, R.; Bletzinger, K.U.: Isogeometric shape optimization of shells using semi-analytical sensitivity analysis and sensitivity weighting. Computer Methods in Applied Mechanics and Engineering, 274, 148–167, 2014. http://doi.org/10.1016/j.cma.2014.02.001.

[22] Lei, Z.; Gillot, F.; Jezequel, L.: Shape optimization for natural frequency with isogeometric Kirchhoff-Love shell and sensitivity mapping. Mathematical Problems in Engineering, 2018(1), 9531651, 2018. http://doi.org/10.1155/2018/9531651.

[23] Lian, H.; Kerfriden, P.; Bordas, S.: Shape optimization directly from CAD: An isogeometric boundary element approach using T-splines. Computer Methods in Applied Mechanics and Engineering, 317, 1–41, 2017. http://doi.org/10.1016/j.cma.2016.11.012.

[24] López, J.; Anitescu, C.; Rabczuk, T.: Isogeometric structural shape optimization using automatic sensitivity analysis. Applied Mathematical Modelling, 89, 1004–1024, 2021. http://doi.org/10.1016/j.apm.2020.07.027.

[25] López, J.; Anitescu, C.; Valizadeh, N.; Rabczuk, T.; Alajlan, N.: Structural shape optimization using Bézier triangles and a CAD-compatible boundary representation. Engineering with Computers, 36, 1657–1672, 2020. http://doi.org/10.1007/s00366-019-00788-z.

[26] Miller, B.; Ziemiański, L.: Maximization of eigenfrequency gaps in a composite cylindrical shell using genetic algorithms and neural networks. Applied Sciences, 9(13), 2754, 2019. http://doi.org/10.3390/app9132754.

[27] Nagy, A.P.; Abdalla, M.M.; Gürdal, Z.: Isogeometric sizing and shape optimisation of beam structures. Computer Methods in Applied Mechanics and Engineering, 199(17-20), 1216–1230, 2010. http://doi.org/10.1016/j.cma.2009.12.010.

[28] Nagy, A.P.; Abdalla, M.M.; Gürdal, Z.: Isogeometric design of elastic arches for maximum fundamental frequency. Structural and Multidisciplinary Optimization, 43, 135–149, 2011. http://doi.org/10.1007/s00158-010-0549-z.

[29] Pan, Q.; Zhai, X.; Kang, H.; Du, X.; Chen, F.: Isogeometric topology optimization of multi-patch shell structures. Computer-Aided Design, 103733, 2024. http://doi.org/10.1016/j.cad.2024.103733.

[30] Sederberg, T.W.; Zheng, J.; Bakenov, A.; Nasri, A.: T-splines and T-NURCCs. ACM transactions on graphics (TOG), 22(3), 477–484, 2003. http://doi.org/10.1145/882262.882295.

[31] Svanberg, K.: A class of globally convergent optimization methods based on conservative convex separable approximations. SIAM Journal on Optimization, 12(2), 555–573, 2002. http://doi.org/10.1137/S1052623499362822.

[32] Videla, J.; Shaaban, A.M.; Atroshchenko, E.: Adaptive shape optimization with NURBS designs and PHT-splines for solution approximation in time-harmonic acoustics. Computers & Structures, 290, 107192, 2024. http://doi.org/10.1016/j.compstruc.2023.107192.

[33] Wall, W.A.; Frenzel, M.A.; Cyron, C.: Isogeometric structural shape optimization. Computer methods in applied mechanics and engineering, 197(33-40), 2976–2988, 2008. http://doi.org/10.1016/j.cma.2008.01.025.

[34] Wang, W.; Jiaming, Y.; Du, X.; Zhang, P.; Han, P.; Liu, Y.; Zhao, G.: Isogeometric shape and topology optimization of Kirchhoff-Love shell structures using analysis-suitable unstructured T-splines. Computer-Aided Design & Applications, 22, 245–260, 2025. http://doi.org/10.14733/cadaps.2025.245-260.

[35] Wang, Y.; Benson, D.J.: Isogeometric analysis for parameterized LSM-based structural topology optimization. Computational Mechanics, 57, 19–35, 2016. http://doi.org/10.1007/s00466-015-1219-1.

[36] Wang, Y.; Wang, Z.; Xia, Z.; Poh, L.H.: Structural design optimization using isogeometric analysis: a comprehensive review. Computer Modeling in Engineering & Sciences, 117(3), 455–507, 2018. http://doi.org/10.31614/cmes.2018.04603.

[37] Weeger, O.: Isogeometric sizing and shape optimization of 3d beams and lattice structures at large deformations. Structural and Multidisciplinary Optimization, 65(2), 43, 2022. http://doi.org/10.1007/s00158-021-03131-7.

[38] Wen, Z.; Pan, Q.; Zhai, X.; Kang, H.; Chen, F.: Adaptive isogeometric topology optimization of shell structures based on PHT-splines. Computers & Structures, 305, 107565, 2024. http://doi.org/10.1016/j.compstruc.2024.107565.

[39] Xu, M.; Wang, S.; Xie, X.: Level set-based isogeometric topology optimization for maximizing fundamental eigenfrequency. Frontiers of Mechanical Engineering, 14, 222–234, 2019. http://doi.org/10.1007/s11465-019-0534-1.

[40] Yang, F.; Yu, T.; Liu, Z.; Bui, T.Q.: Isogeometric double-objective shape optimization of free-form surface structures with Kirchhoff–Love shell theory. Finite Elements in Analysis and Design, 223, 103989, 2023. http://doi.org/10.1016/j.finel.2023.103989.

[41] Yin, S.; Huang, J.; Zou, Z.; Bui, T.Q.; Cong, Y.; Yu, T.; Zhang, G.: Isogeometric shape optimization for widening band gaps of periodic composite plates. European Journal of Mechanics-A/Solids, 103, 105142, 2024. http://doi.org/10.1016/j.euromechsol.2023.105142.

[42] Zhang, W.; Li, D.; Kang, P.; Guo, X.; Youn, S.K.: Explicit topology optimization using IGA-based moving morphable void (MMV) approach. Computer Methods in Applied Mechanics and Engineering, 360, 112685, 2020. http://doi.org/10.1016/j.cma.2019.112685.

[43] Zhang, Z.; Yu, H.; Wu, H.; Chen, Q.: A simultaneous shape and topology optimization approach of shell structures based on isogeometric analysis and density distribution field. Computers & Structures, 305, 107550, 2024. http://doi.org/10.1016/j.compstruc.2024.107550.

[44] Zhao, H.; Kamensky, D.; Hwang, J.T.; Chen, J.S.: Automated shape and thickness optimization for non-matching isogeometric shells using free-form deformation. Engineering with Computers, 1–24, 2024. http://doi.org/10.1007/s00366-024-01947-7.

[45] Zhou, Z.; Sun, Y.; Li, X.; Zhou, Y.; Tian, K.; Hao, P.; Wang, B.: Shape and size optimization framework of stiffened shell using isogeometric analysis. Thin-Walled Structures, 204, 112311, 2024. http://doi.org/10.1016/j.tws.2024.112311.